

Exploiting GPU/SIMD Architectures for Solving Linear-Quadratic MPC Problems*

David Cole,¹ Sungho Shin,² François Pacaud,² Victor M. Zavala,^{1,2} Mihai Anitescu^{2,3}

Abstract—We report numerical results on solving constrained linear-quadratic model predictive control (MPC) problems by exploiting graphics processing units (GPUs). The presented method reduces the MPC problem by eliminating the state variables and applies a condensed-space interior-point method to remove the inequality constraints in the KKT system. The final condensed matrix is positive definite and can be efficiently factorized in parallel on GPU/SIMD architectures. In addition, the size of the condensed matrix depends only on the number of controls in the problem, rendering the method particularly effective when the problem has many states but few inputs and moderate horizon length. Our numerical results for PDE-constrained problems show that the approach is an order of magnitude faster than a standard CPU implementation. We also provide an open-source Julia framework that facilitates modeling (`DynamicNLPModels.jl`) and solution (`MadNLP.jl`) of MPC problems on GPUs.

I. INTRODUCTION

The fundamental challenge of model predictive control (MPC) is solving optimal control (dynamic optimization) problems within short sample time intervals. The real-time computation load can be prohibitive, especially when the system dimension is high or the prediction horizon is long; such computational challenges have limited the application scope of MPC. Accordingly, the scalable solution of optimal control problems has been a long-standing challenge in MPC, with gradual improvements being made to the algorithm [1]–[7].

While numerical solvers have greatly improved thanks to strides in algorithms and computing hardware, the performance of single-core processors has started to stall in the past decade. Rather, progress in hardware has been primarily driven by parallel architectures such as multicore processors, distributed computing clusters, and graphics processing units (GPUs). Hence, in order to continue leveraging advances in modern computing hardware, algorithms and software implementations that harness such capabilities must be developed. While the use of multicore processors and distributed computing has been widely studied in the field of mathematical optimization [8]–[11], relatively fewer contributions have been made regarding the use of GPUs and, more specifically, the use of single instruction, multiple-data (SIMD) architectures. In this context, our work is devoted to

accelerating the solution of linear-quadratic MPC problems by exploiting modern GPU/SIMD architectures.

Developing algorithms for MPC problems on GPU/SIMD architectures offers another benefit for embedded applications (e.g., robotics and autonomous vehicles), in addition to reducing the solution time. The embedded systems with GPU/SIMD capabilities, such as NVIDIA Jetson or the BeagleBoard X15, have the potential to decrease energy use, as compared with CPUs [12]. Accordingly, they allow the potential to create new applications for embedded systems [13], [14]. The use of such embedded systems for MPC has been reported in recent works [15]–[17].

The efficient solution of MPC problems (on either CPUs or GPUs) requires tailored linear algebra techniques that exploit the structure of the Karush–Kuhn–Tucker (KKT) systems arising in the optimization procedure. Classical linear algebra methods include Riccati-like recursions [3], sparse LU factorizations [4], or sparse LDL^T factorizations [18]. These methods rely on direct linear solvers that exploit the sparsity or the block tridiagonal structure of the KKT systems. Despite being highly efficient on CPUs, most sparse matrix factorization routines are sequential and known to be difficult to parallelize. Furthermore, when the factorization of the sparse matrix requires a lot of fill-ins (e.g., as in PDE systems [19]), the sparse direct solver can become extremely slow.

An alternative approach to sparse methods is to formulate the problem in a reduced space by eliminating the state variables. This is readily done by writing each state as a function of the initial state and the previous controls [6] (*reduction*). By further eliminating the inequality constraints using a Schur complement technique (*condensation*), the Newton step computation can be performed by solving a small (the only variables are controls) positive definite system, which can be factorized efficiently with dense Cholesky. Jerez et al. [6] highlight this method and compare the computational complexity of the step computation within sparse and dense methods. Their complexity analysis suggests that the dense method is particularly effective when the number of states is large, the number of controls is small, and the time horizon is short. We note that the dense formulation has been used in various contexts [5], [20], [21] and is implemented in the state-of-the-art MPC solver HPIPM [22].

All these methods transpose directly in the linear algebra routine employed inside the optimization solver and can be exploited in conjunction with a GPU-accelerated interior-point method (IPM) [4], [23]–[27]. Indeed, in direct contrast to active-set methods (which imply expensive reordering operations in the KKT systems, associated with changes

*This material is based upon work supported by the U.S. Department of Energy, Office of Science, Office of Advanced Scientific Computing Research (ASCR) under Contract DE-AC02-06CH11347.

¹Department of Chemical and Biological Engineering, University of Wisconsin-Madison, Madison, WI 53706

²Mathematics and Computer Science Division, Argonne National Laboratory, Lemont, IL 60439

³Department of Statistics, University of Chicago, Chicago, IL 60637

in the active set), IPM involves the solution of a sequence of KKT systems with a fixed sparsity pattern. Hence, the computational burden lies primarily at the linear algebra level (i.e., parallelizing IPM requires solving KKT systems in parallel). To overcome the limitations of sparse direct indefinite factorization routines on GPUs [28], attempts to solve IPM on GPUs have relied on alternative linear algebra routines such as iterative methods [24], CPU-GPU methods [23], or reduction methods [27]. In the context of MPC, Gade-Nielsen and co-workers [29], [30] developed an algorithm and implementation for solving linear programs for MPC (LP-MPC) by factorizing the matrix on a GPU. In their case study, they reported an order of magnitude speedup on the GPU as their problem scale increased. Lee et al. [4] applied an IPM to the standard linear-quadratic MPC formulation with sparse LU factorizations on the GPU. Their method resulted in speedups of a factor of 3–4 over an alternative implementation on the CPU.

A different approach for implementing optimization algorithms on GPU/SIMD architectures is to use iterative linear solvers. Recently, a new algorithm for general quadratic programs (QPs) based on the operator-splitting technique has been proposed [31]. The technique eliminates the necessity to factorize the KKT system in each iteration and greatly accelerates the solution. The algorithm was subsequently adapted for GPUs by replacing the initial sparse factorization step (difficult to parallelize) with an iterative method (in particular, preconditioned conjugate gradient method) [32]. It has been reported that more than 10 times speedup can be made through GPU accelerations [32].

Our goal is to demonstrate the capability of modern GPU architectures for solving dense linear-quadratic MPC problems. We formulate the problem by applying the reduction method presented in [6] and applying the condensed-space interior-point method with dense Cholesky factorization routines within the CUDA library.¹ To the best of our knowledge, this is the first implementation of condensed-space IPM running on GPU for solving linear-quadratic MPC problems and with the potential to be extended to nonlinear MPC. The *dense problem formulation* is implemented in the modeling library `DynamicNLPModels.jl`, and the *condensation* is implemented in the nonlinear optimization solver `MadNLP.jl`. The proposed method is demonstrated by using case studies for PDE-constrained optimal control problems. Our results show that solving dense problems using the GPU can offer an order of magnitude speedup.

¹We highlight that state elimination (*reduction to a dense formulation*) is performed before solving the problem and that the inequality elimination (*condensation*) is performed internally within the interior-point solver when formulating the linear system for the step computations.

II. DENSE FORMULATION

We consider the following linear-quadratic MPC problem:

$$\min_{\substack{\{x_t\}_{t=0}^T, \\ \{u_t\}_{t=0}^{T-1}}} x_T^\top Q_f x_T + \sum_{t=0}^{T-1} \begin{bmatrix} x_t \\ u_t \end{bmatrix}^\top \begin{bmatrix} Q & S \\ S^\top & R \end{bmatrix} \begin{bmatrix} x_t \\ u_t \end{bmatrix} \quad (1a)$$

$$\text{s.t. } x_0 = \bar{x}, \quad (1b)$$

$$x_{t+1} = Ax_t + Bu_t + w_t \quad \forall t \in \mathbb{I}_{[0, T-1]} \quad (1c)$$

$$g^l \leq Ex_t + Fu_t \leq g^u \quad \forall t \in \mathbb{I}_{[0, T-1]} \quad (1d)$$

$$x^l \leq x_t \leq x^u \quad \forall t \in \mathbb{I}_{[0, T]} \quad (1e)$$

$$u^l \leq u_t \leq u^u \quad \forall t \in \mathbb{I}_{[0, T-1]}, \quad (1f)$$

where $x_t \in \mathbb{R}^{n_x}$ are the states at time t , $u_t \in \mathbb{R}^{n_u}$ are the inputs at time t , \bar{x} is the initial known state, and T is the number of steps in the time horizon. Here $x^l, x^u, w_t \in \mathbb{R}^{n_x}$, $u^l, u^u \in \mathbb{R}^{n_u}$, $g^l, g^u \in \mathbb{R}^{n_c}$, $A \in \mathbb{R}^{n_x \times n_x}$, $B \in \mathbb{R}^{n_x \times n_u}$, $Q, Q_f \in \mathbb{R}^{n_x \times n_x}$, $R \in \mathbb{R}^{n_u \times n_u}$, $S \in \mathbb{R}^{n_x \times n_u}$, $E \in \mathbb{R}^{n_c \times n_x}$, $F \in \mathbb{R}^{n_c \times n_u}$ are problem data. We use n_x for the number of states, n_u for the number of inputs, and n_c for the number of constraints in Equation (1d).

The dense form of (1) can be derived by eliminating the state variables. The detailed procedure can be found in [6]; here we outline the key ideas. First, to allow compact notation, we let $\mathbf{x} := [x_0^\top, x_1^\top, \dots, x_T^\top]^\top$, $\mathbf{u} := [u_0^\top, u_1^\top, \dots, u_{T-1}^\top]^\top$, and $\mathbf{w} := [w_0^\top, w_1^\top, \dots, w_{T-1}^\top]^\top$. For inducing the sparsity (when (A, B) is controllable) and for the numerical stability in the elimination procedure (note that the power of A diverges quickly if A is unstable), we introduce a new variable v_t with stabilizing feedback K by

$$u_t = Kx_t + v_t \quad \forall t \in \mathbb{I}_{[0, T-1]}, \quad (2)$$

and we let $A_K := A + BK$ and $\mathbf{v} := [v_0^\top, v_1^\top, \dots, v_{T-1}^\top]^\top$. After the elimination of the state variables, the dynamic constraint (1c) reduces to

$$\mathbf{x} = \mathbf{A}\bar{x} + \mathbf{B}\mathbf{v} + \tilde{\mathbf{A}}\mathbf{w}, \quad (3)$$

where \mathbf{A} , $\tilde{\mathbf{A}}$, and \mathbf{B} are defined as

$$\mathbf{A} := \begin{bmatrix} I_n \\ A_K \\ A_K^2 \\ \vdots \\ A_K^{T-1} \\ A_K^T \end{bmatrix}, \quad \tilde{\mathbf{A}} := \begin{bmatrix} I_n & & & & \\ A_K & I_n & & & \\ \vdots & & \ddots & & \\ A_K^{T-2} & A_K^{T-3} & & & I_n \\ A_K^{T-1} & A_K^{T-2} & \dots & A_K & I_n \end{bmatrix}$$

$$\mathbf{B} := \begin{bmatrix} B & & & & \\ A_K B & B & & & \\ \vdots & & \ddots & & \\ A_K^{T-2} B & A_K^{T-3} B & & B & \\ A_K^{T-1} B & A_K^{T-2} B & \dots & A_K B & B \end{bmatrix}.$$

By substituting (2) and (3) into (1), we obtain the dense MPC problem:

$$\min_{\mathbf{v}} \frac{1}{2} \mathbf{v}^\top \mathbf{H} \mathbf{v} + \mathbf{h}^\top \mathbf{v} + \mathbf{h}_0 \quad (4a)$$

$$\text{s.t. } \mathbf{J} \mathbf{v} \leq \mathbf{d}, \quad (4b)$$

where \mathbf{H} , \mathbf{J} , \mathbf{h} , \mathbf{h}_0 , and \mathbf{d} are defined implicitly by the elimination procedure.

Observe that the problem is expressed only in terms of \mathbf{v} . This dense formulation has Tn_u variables and $2T(n_c + n_x + n_u)$ inequality constraints. Thus, the number of variables is significantly reduced, but now the problem has dense Hessian \mathbf{H} and Jacobian \mathbf{J} . By exploiting the controllability, one can partially maintain the sparsity; for more details on the state elimination procedure, readers are pointed to [6].

III. CONDENSED-SPACE INTERIOR-POINT METHOD

We now describe the condensed-space IPM applied to the dense MPC problem in (4). First, we reformulate (4) by introducing the slack variable \mathbf{s} :

$$\min_{\mathbf{v}, \mathbf{s}} \frac{1}{2} \mathbf{v}^\top \mathbf{H} \mathbf{v} + \mathbf{h}^\top \mathbf{v} + \mathbf{h}_0 \quad (5a)$$

$$\text{s.t. } \mathbf{J} \mathbf{v} - \mathbf{d} + \mathbf{s} = 0 \quad (5b)$$

$$\mathbf{s} \geq 0. \quad (5c)$$

The IPM treats the inequality constraints by replacing the inequality (5c) by the log barrier function $-\mu \sum_{i=1}^m \log(s_i)$, where μ is the barrier term and s_i is the i th value of \mathbf{s} . The resulting barrier subproblem has the form

$$\min_{\mathbf{v}, \mathbf{s}} \frac{1}{2} \mathbf{v}^\top \mathbf{H} \mathbf{v} + \mathbf{h}^\top \mathbf{v} + \mathbf{h}_0 - \mu \sum_{i=1}^m \log(s_i) \quad (6a)$$

$$\text{s.t. } \mathbf{J} \mathbf{v} - \mathbf{d} + \mathbf{s} = 0. \quad (6b)$$

The resulting KKT conditions are then

$$\mathbf{H} \mathbf{v} + \mathbf{h} + \mathbf{J}^\top \boldsymbol{\lambda} = 0 \quad (7a)$$

$$\boldsymbol{\lambda} - \mathbf{z} = 0 \quad (7b)$$

$$\mathbf{J} \mathbf{v} - \mathbf{d} + \mathbf{s} = 0, \quad (7c)$$

where $\mathbf{z} := \mu \mathbf{S}^{-1} \mathbf{1}$, $\boldsymbol{\lambda}$ is the Lagrange multiplier of (6b), $\mathbf{S} := \text{diag}(\mathbf{s})$, and $\mathbf{1}$ is the vector of ones.

Typical IPMs compute the step direction by applying Newton's method to the primal-dual equation in (7). The step computation involves the solution of linear systems of the following form:

$$\begin{bmatrix} \mathbf{H} & \mathbf{J}^\top \\ \mathbf{J} & \mathbf{I} \end{bmatrix} \begin{bmatrix} \mathbf{p}^v \\ \mathbf{p}^s \\ \mathbf{p}^\lambda \end{bmatrix} = - \begin{bmatrix} \mathbf{r}_1 \\ \mathbf{r}_2 \\ \mathbf{r}_3 \end{bmatrix} \quad (8)$$

where \mathbf{p}^v , \mathbf{p}^s , and \mathbf{p}^λ are the descent directions for \mathbf{v} , \mathbf{s} , and \mathbf{z} , respectively; $\mathbf{r}_1 := \mathbf{H} \mathbf{v} + \mathbf{h} + \mathbf{J}^\top \boldsymbol{\lambda}$, $\mathbf{r}_2 := \boldsymbol{\lambda} - \mu \mathbf{S}^{-1} \mathbf{1}$, $\mathbf{r}_3 := \mathbf{J} \mathbf{v} - \mathbf{d} + \mathbf{s}$; and $\boldsymbol{\Sigma}_s := \mathbf{S}^{-1} \mathbf{Z}$ with $\mathbf{Z} := \text{diag}(\mathbf{z})$. Note that this requires that \mathbf{S} be invertible, but this is always the case in IPMs because the primal iterate always stays in the strict interior $\mathbf{s} > 0$.

This KKT system can be further condensed by writing \mathbf{p}^λ as a function of \mathbf{p}^s and \mathbf{p}^s as a function of \mathbf{p}^v . We then obtain a system of equations for \mathbf{p}^v :

$$\left(\mathbf{H} + \mathbf{J}^\top \boldsymbol{\Sigma}_s \mathbf{J} \right) \mathbf{p}^v = -\mathbf{r}_1 + \mathbf{J} \mathbf{r}_2 - \mathbf{J}^\top \boldsymbol{\Sigma}_s \mathbf{r}_3. \quad (9)$$

Here, $\mathbf{H} + \mathbf{J}^\top \boldsymbol{\Sigma}_s \mathbf{J}$ is positive definite and can be factorized with the Cholesky factorization, and \mathbf{p}^v can be computed

Algorithm 1 Condensed-space interior-point method

Require: A, B, Q, R, S, K, N, x_0

Construct \mathbf{H} , \mathbf{h} , \mathbf{h}_0 , \mathbf{J} , and \mathbf{d}

Initialize $\mathbf{v}^{(0)}$, $\mathbf{s}^{(0)}$, and $\boldsymbol{\lambda}^{(0)}$

while Termination criteria are not met **do**

$$\boldsymbol{\Sigma}_s^{(k)} \leftarrow (\mathbf{S}^{(k)})^{-1} \mathbf{Z}^{(k)}$$

$$\text{Compute } \mathbf{H} + \mathbf{J}^\top \boldsymbol{\Sigma}_s^{(k)} \mathbf{J}$$

Factorize $\mathbf{H} + \mathbf{J}^\top \boldsymbol{\Sigma}_s^{(k)} \mathbf{J}$ and solve (9) for $\mathbf{p}^{v(k)}$.

$$\mathbf{p}^{s(k)} \leftarrow -\mathbf{r}_3 - \mathbf{J} \mathbf{p}^{v(k)}$$

$$\mathbf{p}^{\lambda(k)} \leftarrow -\mathbf{r}_2 + \boldsymbol{\Sigma}_s \mathbf{r}_3 + \boldsymbol{\Sigma}_s \mathbf{J} \mathbf{p}^{v(k)}$$

$$\mathbf{p}^{z(k)} \leftarrow \mu \mathbf{S}^{-1} \mathbf{1} - \mathbf{z}^{(k)} - \boldsymbol{\Sigma} \mathbf{p}^{s(k)}$$

Determine the step length α , α_z through line search

$$\mathbf{v}^{(k)} \leftarrow \mathbf{v}^{(k)} + \alpha \mathbf{p}^{v(k)}$$

$$\mathbf{s}^{(k)} \leftarrow \mathbf{s}^{(k)} + \alpha \mathbf{p}^{s(k)}$$

$$\boldsymbol{\lambda}^{(k)} \leftarrow \boldsymbol{\lambda}^{(k)} + \alpha \mathbf{p}^{\lambda(k)}$$

$$\mathbf{z}^{(k)} \leftarrow \mathbf{z}^{(k)} + \alpha_z \mathbf{p}^{z(k)}$$

end while

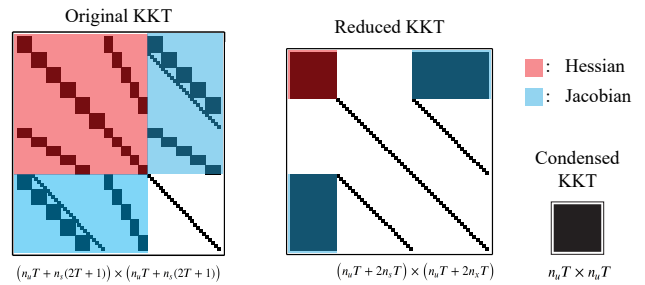


Fig. 1. Full, reduced, and condensed system for linear-quadratic MPC problems.

by back triangular solve. Once \mathbf{p}^v is obtained, \mathbf{p}^s can be obtained from $\mathbf{p}^s = -\mathbf{r}_3 - \mathbf{J} \mathbf{p}^v$, and \mathbf{p}^λ can be found from $\mathbf{p}^\lambda = -\mathbf{r}_2 + \boldsymbol{\Sigma}_s \mathbf{r}_3 + \boldsymbol{\Sigma}_s \mathbf{J} \mathbf{p}^v$. After the descent directions have been determined, a backtracking line search is performed to determine the step size, and the next iterate is obtained based on the step size and the direction. The new values of \mathbf{v} , \mathbf{s} , and \mathbf{z} at the end of this process are then used in the next iteration, and the process is continued until a stopping criterion is satisfied. The method is summarized in Algorithm 1; here, the superscript (k) represents the iterate at k th iteration.

The system in (9) is (i) smaller ($n_u T$ rows and columns) than the system in (8) ($n_u T + 2(n_c + n_x + n_u)T$ rows and columns), (ii) dense, and (iii) positive definite. These features make it more efficient to perform Algorithm 1 on the GPU or other parallel architecture because the Cholesky factorization of small dense systems can be easily parallelized, and efficient implementation is available within the CUDA library. An illustration of the sparsity pattern of full, reduced, and condensed KKT systems with one-sided bounds on the state variables is shown in Figure 1 (for $n_x = 5$, $n_u = 3$, $n_c = 0$, and $T = 5$).

IV. IMPLEMENTATION

To facilitate building and solving sparse or reduced linear-quadratic MPC problems, we have developed the Julia package `DynamicNLPModels.jl`. This package takes data given in (1) and builds either the sparse or reduced forms of these problems. The package is open source, and the source code can be found at [33]. Further, the model returned by `DynamicNLPModels.jl` is a subtype of the generic NLP model data structure implemented in `NLPModels.jl` [34] and so is compatible with other solvers in the `JuliaSmoothOptimizer` ecosystem. By building the reduced problem outside the solver, `DynamicNLPModels.jl` facilitates forming the reduced KKT system (8), which can then be further condensed (9) as the system in (9) within `MadNLP.jl`.

`DynamicNLPModels.jl` allows the user to easily define either the sparse (Equation (1)) or reduced (Equation (4)) linear-quadratic MPC problem by passing user-defined data. An example of how these models are built can be seen in the code snippet below.

```
using DynamicNLPModels
using Random, LinearAlgebra

Q = 1.5 * Matrix(I, (3, 3))
R = 2.0 * Matrix(I, (2, 2))
A = rand(3, 3)
B = rand(3, 2)
T = 5
s0 = [1.0, 2.0, 3.0]

sparse_lqdm =
  SparseLQDynamicModel(s0, A, B, Q, R, T)
dense_lqdm =
  DenseLQDynamicModel(s0, A, B, Q, R, T)
```

The sparse and reduced models can be constructed by passing the user-defined data to `SparseLQDynamicModel` or `DenseLQDynamicModel`. For the dynamic model constructors, keyword arguments can also be passed for the data given in Equations (1) and (2), including Q_f , S , K , E , F , x^l , x^u , u^l , u^u , w , g^l , and g^u .

V. NUMERICAL RESULTS

We apply the condensed-space IPMs to a 3-D PDE temperature control problem to showcase the potential benefits and limitations of our approach. For problems with low numbers of inputs and high numbers of constraints, we show that solving the dense linear-quadratic MPC problem on the GPU using a condensed-space IPM can offer an order of magnitude speedup over solving the dense problem on the CPU with the condensed-space IPM or solving the sparse problem on the CPU. Also, our results suggest that the condensed-space GPU approach is less effective for problems with a low ratio of states to inputs. In all cases, we constructed the model using `DynamicNLPModels.jl`. We solved the sparse form of the problem using `Ipopt` [35] with `MA27` [18] as the linear solver. We solved the dense form of the problem on the CPU as well as the GPU using `MadNLP.jl` and dense Cholesky factorization using

TABLE I

PARAMETER VALUES FOR THE 3-D TEMPERATURE CONTROL PROBLEM.

Δ_t	Temporal discretization mesh size	0.1 sec
Δ_w	Spatial discretization mesh size	0.02 m
L	Length of cube face	$(N+1)\Delta_w$
ρ	Density of copper	8960 kg · m ⁻³
C_p	Specific heat of copper	386 J · (kg · K) ⁻¹
k	Thermal conductivity of copper	400 W · (m · K) ⁻¹
q	Weight on temperature error	$10 \Delta_w^2$ m ⁻²
r	Weight on input	$\frac{1}{10} \Delta_w^2$ m ⁻²
(x^l, x^u)	(Lower, upper) temperature bounds	(200, 550) K
(u^l, u^u)	(Lower, upper) input bounds	(300, 500) K
\hat{x}	Initial temperature	300 K

LAPACK (OpenBLAS) or CUSOLVER. Scripts and solver outputs are available at [36].

A. Problem Formulation

We adapted the 2-D thin plate temperature control problem given by [7] to a 3-D temperature control problem in a cube using the boundary inputs. In this problem, each face of the cube can be heated by control to try to reach the desired temperature profile. The continuous form of this problem can be stated as follows:

$$\min_{x,u} \frac{1}{2} \int_0^T \int_{w \in \Omega} \left(q(x(w,t) - d(w,t))^2 dw + \sum_{i \in \mathcal{U}} r u_i(t)^2 \right) dt \quad (10a)$$

$$\text{s.t. } \rho C_p \frac{\partial x(w,t)}{\partial t} = k \nabla^2 x(w,t), \quad w \in \Omega, t \in [0, T] \quad (10b)$$

$$x^l \leq x(w,t) \leq x^u \quad w \in \Omega, t \in [0, T] \quad (10c)$$

$$u^l \leq u_i(t) \leq u^u \quad i \in \mathcal{U}, w \in \Omega, t \in [0, T] \quad (10d)$$

$$x(w,t) = u_i(t), \quad i \in \mathcal{U}, w \in \partial\Omega_i, t \in [0, T] \quad (10e)$$

$$x(w,0) = \hat{x}, \quad w \in \Omega, \quad (10f)$$

where $\Omega = [0, L]^3 \subseteq \mathbb{R}^3$ is the 3-D domain of a cube of length L , $\mathcal{U} := \{1, 2, \dots, 6\}$ is the set of all cube faces, $x : \Omega \times [0, T] \rightarrow \mathbb{R}$ is the temperature, $d : \Omega \times [0, T] \rightarrow \mathbb{R}$ is the set point temperature, $u_i : [0, T] \rightarrow \mathbb{R}$ are the boundary temperatures for $i \in \mathcal{U}$, and $\partial\Omega_i \subseteq \Omega$ for $i \in \mathcal{U}$ are the boundaries. Note that (10e) enforces the Dirichlet boundary condition. The constant values are given in Table I.

The infinite-dimensional problem in (10) is discretized by using a finite difference method in space and an explicit Euler scheme in time to make a finite-dimensional MPC problem of the form in (1). We also treat the boundaries as inputs only (not as states), so all of the state variables are strictly internal temperatures. In addition, this problem can be scaled up by changing T (the time horizon) or N (the number of discretization points per dimension). Note that increasing N increases cubically the number of states because the spatial domain is three-dimensional.

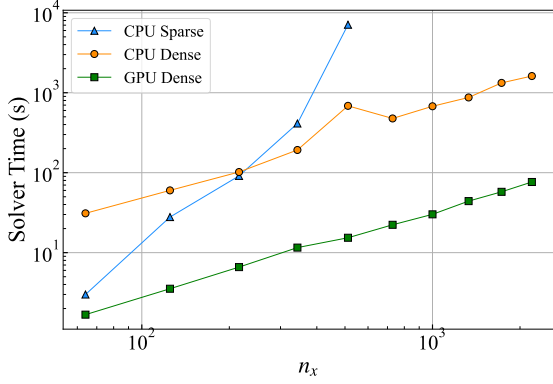


Fig. 2. Total solver time for $T = 250$.

TABLE II
SOLVER STATISTICS FOR $T = 250$ AND VARIED N .

N	CPU Sparse			CPU Dense			GPU Dense		
	iter	tot	lin	iter	tot	lin	iter	tot	lin
4	26	3.0	2.6	28	31.0	1.10	28	1.68	0.037
5	30	27.9	24.8	33	60.1	1.30	33	3.54	0.045
6	29	91.2	81.4	31	102.0	1.25	31	6.59	0.041
7	32	412.3	372.0	38	192.3	1.55	38	11.6	0.055
8	31	7086.	6617.	37	685.4	1.66	37	15.4	0.051
9	-	-	-	38	476.8	1.77	38	22.3	0.056
10	-	-	-	37	677.2	1.76	37	30.1	0.052
11	-	-	-	38	872.6	1.74	38	44.1	0.058
12	-	-	-	38	1328	1.74	38	57.6	0.064
13	-	-	-	39	1617	1.79	39	76.5	0.067

B. Results

We solved problems (i) over a range of N values at three different numbers of time steps: $T = 50$, $T = 150$, and $T = 250$ and (ii) over a range of T values for fixed $N = 4$. The results can be seen in Figures 2 and 3 and Tables II–V. In the tables, “iter” is the number of iterations within IPMs reported by the solvers (Ipopt for the sparse problems and MadNLP.jl for the dense problems), “tot” is the total solver time, and “lin” is the linear solver time.

In all three tests with varying N , solution times increased significantly with N . However, the results indicate that the computation time of the sparse problem grows more rapidly in N compared with the dense problems. The reason is that in the 3-D temperature control problem, the number of variables in the dense problem remains unchanged (the number of inputs is independent of N), whereas the number of variables of the sparse problem scales cubically in N . Note that problems with rapidly growing numbers of states can easily arise in discretized PDE-constrained control problems. Also, because of the structure of the discretization of 3-D PDEs, the fill-ins in the factorization grow rapidly, and the sparse solver becomes inefficient as N grows. Although the number of variables in the condensed-space approaches does not change, the solution time is moderately affected by N . The reason is that the number of constraints increases with N , making the number of rows in the Jacobian grow linearly with N . While the dense system size is still independent of

TABLE III
SOLVER STATISTICS FOR $T = 150$ AND VARIED N .

N	CPU Sparse			CPU Dense			GPU Dense		
	iter	tot	lin	iter	tot	lin	iter	tot	lin
4	25	1.7	1.4	27	8.90	0.31	27	0.68	0.022
5	29	17.2	15.4	32	17.4	0.54	32	1.26	0.028
6	29	55.9	49.9	31	28.9	0.37	31	1.93	0.027
7	30	238.2	214.1	36	53.0	0.43	36	4.19	0.034
8	31	4,953.	4,636.	37	155.5	0.45	37	6.12	0.034
9	31	10,357.	9,703.	38	110.5	0.40	38	8.05	0.034
10	-	-	-	36	153.2	0.39	36	10.8	0.034
11	-	-	-	38	221.1	0.43	38	15.1	0.037
12	-	-	-	38	353.7	0.48	38	18.9	0.040
13	-	-	-	39	404.1	0.50	39	25.2	0.045
14	-	-	-	40	559.6	0.53	40	32.6	0.045

TABLE IV
SOLVER STATISTICS FOR $T = 50$ AND VARIED N .

N	CPU Sparse			CPU Dense			GPU Dense		
	iter	tot	lin	iter	tot	lin	iter	tot	lin
4	26	0.6	0.5	27	0.45	0.020	27	0.09	0.008
5	28	5.0	4.4	32	1.01	0.023	32	0.17	0.009
6	27	17.5	15.5	29	1.66	0.022	29	0.23	0.008
7	27	69.1	61.4	33	3.36	0.024	33	0.41	0.010
8	32	689.0	641.1	37	10.1	0.030	37	0.70	0.011
9	30	3,100.	2,936.	37	7.79	0.033	37	0.94	0.011
10	-	-	-	36	9.69	0.033	36	1.71	0.011
11	-	-	-	37	13.9	0.034	37	2.00	0.012
12	-	-	-	37	18.1	0.034	37	2.43	0.012
13	-	-	-	38	22.6	0.035	38	3.37	0.013
14	-	-	-	38	25.6	0.033	38	4.08	0.013

N , the condensation procedure, which involves computing $\mathbf{J}^\top \Sigma_s \mathbf{J}$, is affected by the dimension of \mathbf{J} .

In all three cases of changing N , the dense formulation on the GPU was much faster than the same formulation/algorithm running on the CPU. For $T = 250$, the GPU was on average 22 times faster; for $T = 150$, it was 16 times faster; and for $T = 50$, it was only 7 times faster. It appears that the GPU operates proportionally faster than the CPU on the larger problem sizes, which is not surprising since the parallelizable computations increase with problem size. However, the solution time for the dense formulation increases faster than the sparse solution time for changing T , as can be seen in Figure 3 and Table V. Jerez et al. [6] report that the number of flops for computing an interior-point iteration of the dense formulation is $\mathcal{O}(T^3 n_u^2 (n_u + n_c))$ while the number of flops for the sparse formulation is $\mathcal{O}(T(n_x + n_u)^2 (n_x + n_u + n_c))$. Thus, even though the number of flops for the sparse formulation goes as $\mathcal{O}(n_x^3)$, the sparse formulation can overtake the dense formulation (on either the CPU or GPU) since the dense formulation goes as $\mathcal{O}(T^3)$ while the sparse formulation goes only as $\mathcal{O}(T)$. This effect can be seen for $N = 4$ and $T = 500$ (see Figure 3 and Table V).

These results suggest that solving linear-quadratic MPC problems on the GPU using the above methods can reduce the solution times by an order of magnitude for certain cases. This speedup can enable applying MPC to new systems that previously would have been limited by time constraints. The types of problems to which this method can practically be

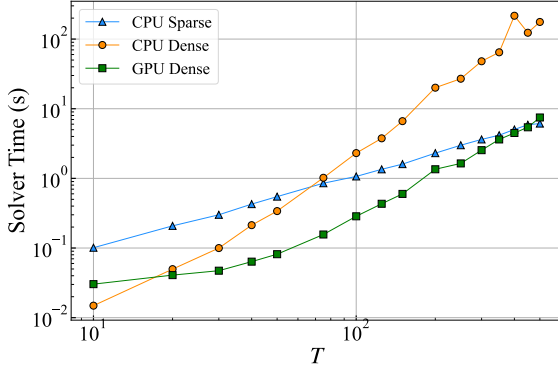


Fig. 3. Total solver time for $N = 4$ and varied T .

TABLE V
SOLVER STATISTICS FOR $N = 4$ AND VARIED T .

T	CPU Sparse			CPU Dense			GPU Dense		
	iter	tot	lin	iter	tot	lin	iter	tot	lin
10	26	0.10	0.079	28	0.02	0.001	28	0.03	0.004
20	25	0.21	0.170	27	0.05	0.002	27	0.04	0.005
30	24	0.30	0.249	26	0.10	0.005	26	0.05	0.005
40	25	0.43	0.356	27	0.21	0.009	27	0.06	0.006
50	26	0.55	0.460	27	0.34	0.016	27	0.08	0.007
75	27	0.85	0.724	29	1.02	0.051	29	0.16	0.010
100	25	1.07	0.900	27	2.31	0.096	27	0.29	0.015
125	25	1.35	1.14	27	3.76	0.162	27	0.43	0.018
150	25	1.60	1.36	27	6.63	0.243	27	0.60	0.021
200	26	2.30	1.97	28	20.0	0.529	28	1.35	0.029
250	26	2.99	2.58	28	27.0	0.979	28	1.64	0.036
300	28	3.63	3.15	30	48.0	1.61	30	2.54	0.047
350	27	4.17	3.61	29	64.6	2.29	29	3.62	0.062
400	27	5.04	4.16	29	216.4	3.30	29	4.48	0.053
450	27	5.89	5.14	29	123.3	4.35	29	5.41	0.067
500	27	6.12	5.30	29	176.2	5.64	29	7.49	0.067

applied are problems with a high ratio of states to inputs and moderate horizon length. As seen above, control systems that can be modeled with PDEs could be one prime candidate. However, our results also suggest that this framework is less effective (and eventually impractical) as the ratio of states to inputs decreases. For example, in Figure 2 the sparse formulation with $N = 4$ is comparable to the GPU solution time and much faster than the dense formulation on the CPU. The reason is that the problem sizes between the sparse and dense formulations are more similar. Numerous linear-quadratic MPC problems have much lower ratios of states to inputs than that of the temperature control problem presented here, and these problems would be less practical in this framework.

VI. CONCLUSIONS AND FUTURE WORK

For problems with large numbers of states and few inputs and moderate horizon length, we can speed up linear-quadratic MPC by an order of magnitude by exploiting the structure using GPU/SMID architectures. We introduced the package `DynamicNLPModels.jl`, which reduces the linear-quadratic MPC problem based on user-defined data. The KKT system of this dense model is a reduced KKT system (as

compared with the sparse formulation), which `MadNLP.jl` automatically constructs when the model is passed from `DynamicNLPModels.jl` to `MadNLP.jl`. The KKT system can be further condensed within `MadNLP.jl`, resulting in a dense positive definite matrix that can be efficiently factorized on the GPU. Based on the example problem of the heating of a cube, this method can result in significant speedup over the dense form or the sparse form on the CPU.

One of the challenges to be addressed in the future is the GPU memory footprint in building the dense problem. The size of the Jacobian is $(n_x + n_u + n_c)T \times n_u T$. This can become prominently large as T and n_x grow. From the definition of \mathbf{J} and \mathbf{B} , however, all the data in \mathbf{J} is found in its first n_u columns, making it possible to store the Jacobian implicitly. This could significantly decrease the memory needed for storing \mathbf{J} . However, building this kernel so that it is competitive with the explicit Jacobian is nontrivial and an area of future work.

REFERENCES

- [1] S. J. Wright, "Partitioned dynamic programming for optimal control," *SIAM Journal on Optimization*, vol. 1, no. 4, pp. 620–642, 1991.
- [2] C. V. Rao, S. J. Wright, and J. B. Rawlings, "Application of interior-point methods to model predictive control," *Journal of Optimization Theory and Applications*, vol. 99, no. 3, pp. 723–757, 1998.
- [3] G. Frison, H. H. B. Sørensen, B. Dammann, and J. B. Jørgensen, "High-performance small-scale solvers for linear model predictive control," in *2014 European Control Conference (ECC)*. IEEE, 2014, pp. 128–133.
- [4] S. Lee, H. Lee, Y. Kim, J. Kim, and W. Choi, "GPU-accelerated PD-IPM for real-time model predictive control in integrated missile guidance and control systems," *Sensors*, vol. 22, no. 12, p. 4512, 2022.
- [5] J. A. Andersson, J. V. Frasch, M. Vukov, and M. Diehl, "A condensing algorithm for nonlinear MPC with a quadratic runtime in horizon length," *Automatica*, pp. 97–100, 2013.
- [6] J. L. Jerez, E. C. Kerrigan, and G. A. Constantinides, "A sparse and condensed QP formulation for predictive control of LTI systems," *Automatica*, vol. 48, no. 5, pp. 999–1002, 2012.
- [7] S. Na, S. Shin, M. Anitescu, and V. M. Zavala, "On the convergence of overlapping Schwarz decomposition for nonlinear optimal control," *IEEE Transactions on Automatic Control*, 2022.
- [8] R. B. Schnabel, "A view of the limitations, opportunities, and challenges in parallel nonlinear optimization," *Parallel Computing*, vol. 21, no. 6, pp. 875–905, 1995.
- [9] S. J. Wright, "Solving optimization problems on computational grids," 2001.
- [10] N. Chiang, C. G. Petra, and V. M. Zavala, "Structured nonconvex optimization of large-scale energy systems using PIPS-NLP," in *2014 Power Systems Computation Conference*. IEEE, 2014, pp. 1–7.
- [11] K. Kim, C. G. Petra, and V. M. Zavala, "An asynchronous bundle-trust-region method for dual decomposition of stochastic mixed-integer programming," *SIAM Journal on Optimization*, vol. 29, no. 1, pp. 318–342, 2019.
- [12] M. Qasaimeh, K. Denolf, J. Lo, K. Vissers, J. Zambreno, and P. H. Jones, "Comparing energy efficiency of CPU, GPU and FPGA implementations for vision kernels," in *2019 IEEE International Conference on Embedded Software and Systems (ICCESS)*, 2019, pp. 1–8.
- [13] T. Dong, V. Dobrev, T. Kolev, R. Rieben, S. Tomov, and J. Dongarra, "A step towards energy efficient computing: Redesigning a hydrodynamic application on CPU-GPU," in *2014 IEEE 28th International Parallel and Distributed Processing Symposium*, 2014, pp. 972–981.
- [14] M. Forgione, D. Piga, and A. Bemporad, "Efficient calibration of embedded MPC," *IFAC-PapersOnLine*, vol. 53, no. 2, pp. 5189–5194, 2020.
- [15] D.-K. Phung, B. Hérisse, J. Marzat, and S. Bertrand, "Model predictive control for autonomous navigation using embedded graphics processing unit," *IFAC-PapersOnLine*, vol. 50, no. 1, pp. 11 883–11 888, 2017.

- [16] K. M. M. Rathai, M. Alamir, and O. Sename, "GPU based stochastic parameterized NMPC scheme for control of semi-active suspension system for half car vehicle," *IFAC-PapersOnLine*, vol. 53, no. 2, pp. 14 369–14 374, 2020.
- [17] L. Yu, A. Goldsmith, and S. Di Cairano, "Efficient convex optimization on GPUs for embedded model predictive control," in *Proceedings of the General Purpose GPUs*. New York, NY, USA: Association for Computing Machinery, 2017, pp. 12–21. [Online]. Available: <https://doi.org/10.1145/3038228.3038234>
- [18] HSL, "A collection of Fortran codes for large scale scientific computation." [Online]. Available: <http://www.hsl.rl.ac.uk/>
- [19] O. Schenk, A. Wächter, and M. Weiser, "Inertia-revealing preconditioning for large-scale nonconvex constrained optimization," *SIAM Journal on Scientific Computing*, vol. 31, no. 2, pp. 939–960, 2009.
- [20] J. B. Rawlings, D. Q. Mayne, and M. Diehl, *Model Predictive Control: Theory, Computation, and Design*. Santa Barbara, CA, USA: Nob Hill Publishing, 2017, ch. 8.
- [21] G. Frison, "Algorithms and methods for high-performance model predictive control," 2016.
- [22] G. Frison and M. Diehl, "HPIPM: a high-performance quadratic programming framework for model predictive control," *IFAC-PapersOnLine*, vol. 53, no. 2, pp. 6563–6569, 2020.
- [23] J. H. Jung and D. P. O'Leary, "Implementing an interior point method for linear programs on a CPU-GPU system," *Electronic Transactions on Numerical Analysis*, vol. 28, no. 174-189, p. 37, 2008.
- [24] E. Smith, J. Gondzio, and J. Hall, "GPU acceleration of the matrix-free interior point method," in *International Conference on Parallel Processing and Applied Mathematics*. Springer, 2011, pp. 681–689.
- [25] Y. Cao, A. Seth, and C. D. Laird, "An augmented lagrangian interior-point approach for large-scale NLP problems on graphics processing units," *Computers & Chemical Engineering*, vol. 85, pp. 76–83, 2016.
- [26] U. A. Shah, S. Yousaf, I. Ahmad, and M. O. Ahmad, "On the efficiency of supernodal factorization in interior-point method using CPU-GPU collaboration," *IEEE Access*, vol. 8, pp. 120 892–120 904, 2020.
- [27] F. Pacaud, S. Shin, M. Schanen, D. A. Maldonado, and M. Anitescu, "Accelerating condensed interior-point methods on SIMD/GPU architectures," *arXiv preprint arXiv:2203.11875*, 2022.
- [28] K. Świrydowicz, E. Darve, W. Jones, J. Maack, S. Regev, M. A. Saunders, S. J. Thomas, and S. Peleš, "Linear solvers for power grid optimization problems: a review of GPU-accelerated linear solvers," *Parallel Computing*, vol. 111, p. 102870, 2022.
- [29] N. F. Gade-Nielsen, J. B. Jørgensen, and B. Dammann, "MPC toolbox with GPU accelerated optimization algorithms," in *10th European workshop on advanced control and diagnosis*. Technical University of Denmark, 2012.
- [30] N. F. Gade-Nielsen, "Interior point methods on GPU with application to model predictive control," 2014.
- [31] B. Stellato, G. Banjac, P. Goulart, A. Bemporad, and S. Boyd, "OSQP: An operator splitting solver for quadratic programs," *Mathematical Programming Computation*, vol. 12, no. 4, pp. 637–672, 2020.
- [32] M. Schubiger, G. Banjac, and J. Lygeros, "GPU acceleration of ADMM for large-scale quadratic programming," *Journal of Parallel and Distributed Computing*, vol. 144, pp. 55–67, 2020. [Online]. Available: <https://doi.org/10.1016/j.jpdc.2020.05.021>
- [33] [Online]. Available: <https://github.com/MadNLP/DynamicNLPModels.jl>
- [34] D. Orban, A. S. Siqueira, and contributors, "NLPModels.jl: Data structures for optimization models," <https://github.com/JuliaSmoothOptimizers/NLPModels.jl>, July 2020.
- [35] A. Wächter and L. T. Biegler, "On the implementation of an interior-point filter line-search algorithm for large-scale nonlinear programming," *Mathematical programming*, vol. 106, no. 1, pp. 25–57, 2006.
- [36] [Online]. Available: https://github.com/dlcole3/3D_temperature_control

Government License: The submitted manuscript has been created by UChicago Argonne, LLC, Operator of Argonne National Laboratory ("Argonne"). Argonne, a U.S. Department of Energy Office of Science laboratory, is operated under Contract No. DE-AC02-06CH11357. The U.S. Government retains for itself, and others acting on its behalf, a paid-up nonexclusive, irrevocable worldwide license in said article to reproduce, prepare derivative works, distribute copies to the public, and perform publicly and display publicly, by or on behalf of the Government. The Department of Energy will provide public access to these results of federally sponsored research in accordance with the DOE Public Access Plan. <http://energy.gov/downloads/doe-public-access-plan>.